THE ELASTIC PLATE THICKNESS AND THE CRUSTAL DENSITY BENEATH THE ELYSIUM VOLCANIC PROVINCE USING THE GMM-3 MARS GRAVITY MODEL

A FINAL REPORT SUBMITTED TO THE DEPARTMENT OF EARTH SCIENCES,
UNIVERSITY OF HAWAI'I AT MĀNOA, IN PARTIAL FULFILLMENT OF THE
REQUIREMENTS FOR THE DEGREE OF

MASTER OF SCIENCE

IN

EARTH AND PLANETARY SCIENCES

DECEMBER 2020

BY

MACKENZIE R. LACH

COMMITTEE:

GARRETT APUZEN-ITO (CHAIR)

NIELS GROBBE

SARAH FAGENTS

Abstract

Much about a planet's crust can be gleaned from observations of its gravity anomalies. The GMM-3 gravity model consolidates 16 years of satellite radio tracking data and reflects an improvement upon the accuracy of previous models, presenting the Martian gravity field to spherical harmonic degree and order 120. This higher resolution allows for improved studies of crustal structure. The Elysium volcanic province is the second-largest on Mars after Tharsis and is home to Elysium Mons, a massive shield volcano rising 14 km above the surrounding region. When large topographic loads such as Elysium Mons form, they cause the lithosphere to flex. This flexure manifests as a broad low in the Bouguer gravity anomaly and contains information about the state of the lithosphere when the load was emplaced. Furthermore, the Bouguer anomaly can reveal crustal density contrasts due to geologic features such as magma chambers. Here, I make use of the GMM-3 gravity model and the Mars Orbiter Laser Altimeter (MOLA) topography to model the flexure of the lithosphere in Cartesian coordinates using Fourier domain filtering. I then predict the Bouguer anomaly by calculating the gravitational effects of the deformation of the crust-mantle boundary, which I then compare to the observed Bouguer anomaly. Numerous calculations assuming different crustal densities and elastic plate thicknesses (T_e) reveal the lowest misfits for densities from $2650\,\mathrm{kg/m^3}$ to $3100\,\mathrm{kg/m^3}$ and T_e ranging from 10 km to 90 km. These ranges of optimal fits are consistent with the values found in the literature. Additionally, an anomaly in the residual Bouguer centered on the peak of Elysium Mons is detected robustly and is consistent with a dense intrusive body that could be the fossil remnant of a magma chamber. Its mass is estimated to be $1.42 \cdot 10^{17}$ kg, with a minimum volume of $1.67 \cdot 10^5$ km^3.

Contents

1 Introduction

1.1 Geology of Mars

When a topographic load is emplaced on the surface of a terrestrial planet, the lithosphere behaves elastically and flexes downwards. The deformation and density contrast associated with the crust-mantle interface produce a flexural signature that is observable in the gravity anomaly. The degree of flexure depends on the height of topography as well as on parameters affecting lithospheric strength at the time the load was emplaced. Once the crust is deformed, the flexure becomes "frozen in" to the state of the crust, thus providing a convenient means of probing the mechanical and thermal history of a planet's crust. On a planet such as Earth, active plate tectonics and crustal recycling throughout its history have periodically reset the crustal age and lithospheric stress state. However, active mantle convection resulting in plate tectonics is currently absent among the other terrestrial bodies in the Solar System, as most are in the stagnant lid regime or have no significant mantle convection altogether [1]. Stagnant lid bodies experience weak or no convection, with only the lower layers of the lithosphere taking part in convection and possessing only one global plate as a result.

Mars is such a stagnant lid planet, and this has had profound implications for its geologic history. Its surface is littered with well over 300,000 impact craters, ranging from kilometer-sized or smaller to the massive Hellas and Utopia basins [2]. In the absence of plate tectonics, these features persist until aeolian or volcanic processes bury or destroy them, allowing for the relative dating of geologic units via cratering statistics (e.g., [3, 2, 4]). The lack of plate tectonics has also allowed for the construction of enormous "supervolcanoes" that number among the largest in the Solar System. While remarkably analogous to Earth's basaltic shields in terms of composition, morphology, and hot-spot provenance (e.g., [5]), Martian volcanoes are far larger than their Earth counterparts. Olympus Mons, the largest volcano in the Solar System, dwarfs both Mount Everest and Mauna Kea and stands at an impressive 22 km above its surrounding terrain. Long-lived hot spots caused by convective plumes in the mantle may be intermittently active over billions of years, erupting material at a single location on the immobile crust and forming extremely large edifices that are not recycled via plate tectonics.

Likewise, the flexural imprints of these volcanoes persist over billions of years, providing a unique window into Mars' entire volcanic history. Effective elastic plate thickness (T_e) represents the bending or flexural strength of the lithosphere that contributes to this flexure. A small T_e is a trademark of a weak, and therefore young, lithosphere. As a terrestrial planet ages and radiates its heat to space, its lithosphere will cool and strengthen, and its T_e will increase. Thus older volcanoes should be expected to have smaller T_e, and younger edifices should have larger T_e [6, 7]. Combined with cratering statistics, flexural modelling of topographic loads is thus a powerful method of studying the thermal evolution and present-day heat flow of the Martian crust (e.g., [8, 9, 7]). It has also been used to estimate ratios of intrusive and extrusive volcanic products [7].

1.2 Gravity Exploration of Mars

Gravity studies provide an excellent means to remotely study the internal density structure of Mars. Radio tracking data from the Mariner 9 and subsequent Viking I

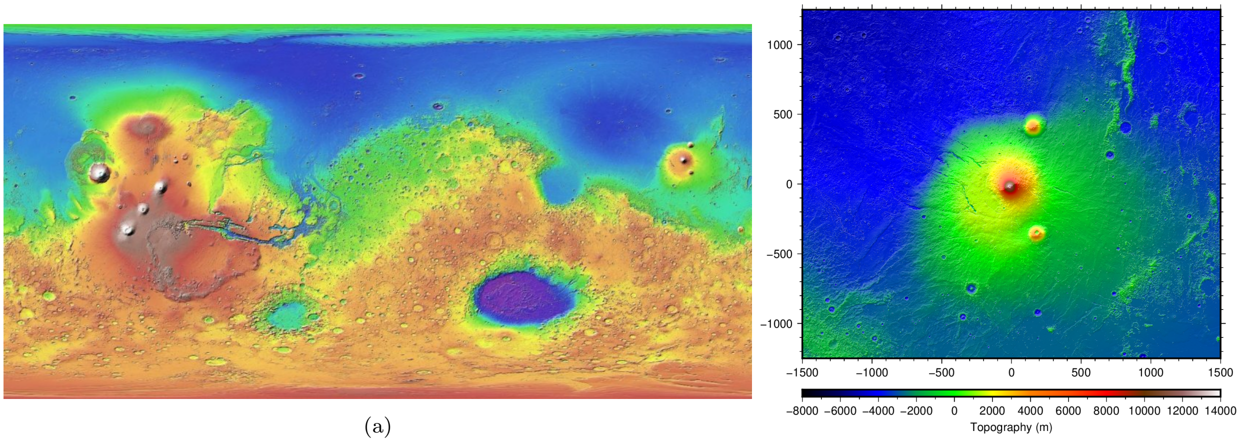

(a)

(b)

Figure 1: (a) Global topography of Mars as measured by MGS MOLA [10]. (b) Isolated MOLA topography of the Elysium Volcanic Province.

and II satellites provided some of the earliest, albeit low resolution, gravity models of Mars (e.g., [11, 12, 13]). More recent satellite missions, such as the Mars Global Surveyor (MGS), Mars Reconnaissance Orbiter (MRO), and Mars Odyssey, have greatly expanded upon this early work and have allowed for the development of far more accurate gravity models [14, 15, 16, 17, 18]. Gravity models allow the calculation of various geodetic parameters, and they also allow for geophysical interpretation of density anomalies. In addition, recent models have uncovered seasonal variability in the Martian gravity field, which is caused primarily by solid tides as well as the cycling of CO_2 between the polar caps and the atmosphere [18]. In planetary studies, gravity models are traditionally expressed as expansions of spherical harmonic coefficients, as this makes it easier to work with global data sets on a sphere. However, Earth studies have typically made use of data that is gridded onto a Cartesian map and then projected back onto a sphere [19]. This introduces some distortion, but is generally suitable for localized studies. Regardless of the chosen coordinate system, analyses can be done either in the spectral or spatial domain. Spectral analyses typically concern the ratio of (i.e., admittance), or the correlation between the gravity and topography power spectra at different spherical harmonic degrees. Admittance and correlation studies are useful for constraining the minimum resolution of a gravity model as well as for inverting for lithosphere parameters [7]. In contrast, spatial analyses compare the predicted and observed gravity anomalies in the spatial domain; this helps facilitate geologic interpretations of the residual anomaly, which is the difference between prediction and observation.

1.3 Elysium Volcanic Province

Located near the edge of the northern lowlands, the Elysium Volcanic Province (Figure 1b) is the second-largest volcanic province after Tharsis. It is situated upon a broad topographic swell, hypothesized to be caused by convective upwelling [20], although it is unclear whether an active plume could still exist [21, 8]. It contains three shield volcanoes, with the largest, Elysium Mons, sitting slightly off-center with a maximum relief of 14 km. The smaller flank volcanoes Hecates and Albor Tholi sit north and south of Elysium Mons, respectively, with reliefs of 5.3 km and 4.2 km. The Elysium Province has had a long and complex eruptive timeline, with activity likely occurring over most of Mars' history [4]. A crater counting study by Platz et al. (2011) [4] of Elysium Mons' caldera and flank lava flows estimated the earliest volcanic activity to have occurred around 3.9 Ga, with the bulk of the activity occurring between 2.5 Ga and 1 Ga, centered at 2.2 Ga. Thus, the bulk of the load was likely emplaced during this time span. After 1 Ga, activity is thought to have decreased significantly, although flows as young as 60 Ma have been identified [4]. The effective elastic thickness of the crust beneath Elysium has been estimated by numerous authors, with typical estimates ranging from 10 km to 50 km [22, 23, 24, 25, 26, 7, 27]. In addition, a previous global study of the Bouguer gravity anomaly has produced evidence for a positive density anomaly relative to Mars' average crustal density that is centered beneath Elysium Mons [28].

In this work, I perform a regional study of the Elysium Volcanic Province using the GMM-3 gravity model to estimate the mean effective elastic plate thickness of the region and to examine density heterogeneity. Analysis is performed in the spatial rather than spectral domain using a Cartesian geometry. I will begin this report by providing an overview of the data sets used in this work, then I will discuss the theory behind flexure calculations, then I will outline my procedure, and finally I will present and discuss my results for the best-fitting elastic plate thicknesses, crustal densities, and geologic interpretation of the residual anomaly.

2 Data

2.1 MOLA Topography

This work makes use of both topographic and gravity data. The most geodetically accurate topographic model of Mars to date is that acquired by the Mars Orbiter Laser Altimeter (MOLA) instrument, which operated as an altimeter aboard MGS until 2001 [10]. A global map of topography is shown in Figure 1a; the resolution at the equator is 1 km in latitude and 2 km in longitude [10]. MOLA topography is referenced from the Martian areoid, which is the equipotential surface with an average equatorial value equal to Mars' average radius at the equator. For this study, the MOLA topography was referenced to the same ellipsoid as the gravity data.

2.2 The GMM-3 Gravity Model

The Goddard Mars Model 3 (GMM-3) was released in 2016 by Genova et al. [18] and is currently the most up-to-date gravity model of Mars. It is calculated up to spherical harmonic degree and order 120, which corresponds to a spatial resolution of 89 km. The GMM-3 model was acquired from 16 years of radio tracking data from the MGS, MRO, and Mars Odyssey missions. As a satellite orbits Mars, variations in the gravity field cause a change in spacecraft acceleration, which is tracked via radio by NASA's Deep Space Network. However, there are many forces other than planet gravity acting upon a spacecraft that influence its motion and must therefore be precisely modelled. The GMM-3 model incorporates highly accurate modelling of non-conservative forces

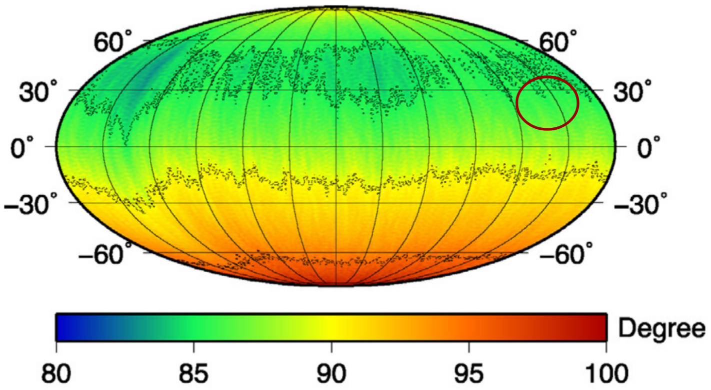

Figure 2: The degree strength map of the GMM-3 model. This represents the maximum degree to which the model is expanded, which is determined to be the degree at which the predicted anomaly at a given point matches its error. From Genova et al. (2016) [18]. At Elysium Mons, circled in dark red, this degree is roughly 85.

such as atmospheric drag, solar and planetary radiation pressure, and momentum wheel desaturation. Spacecraft telemetry data along orbital arcs were combined and processed and then used to invert for the gravity spherical harmonic coefficients [18].

Although the 120 spherical harmonic degree corresponds roughly to a spatial resolution of 89 km, the spherical harmonic degrees that are useful for geophysical interpretation, and thus the minimum resolution, vary across the planet. At lower spherical harmonic degrees, the topography is expected to be locally compensated so that the gravity anomaly is well-correlated with topography. In contrast, at higher degrees regional compensation is expected to reduce the correlation between gravity and topography. Therefore, higher degrees contain critical information about flexure, although they introduce noise and non-physical artifacts. The GMM-3 model has the advantage over earlier models of having better correlation between gravity and topography at higher degrees. Genova et al. (2016) apply the Kaula rule, which states that the gravity coefficients are bounded by a power law [29, 30], to degrees above 90 and use a degree strength approach that determines the maximum spherical harmonic degree at each point to be where the predicted anomaly is equal to its uncertainty [31, 18]. Figure 2 shows globally the maximum degree to which the GMM-3 model can be expanded to according to this constraint. Resolution tends to be better near the southern latitudes; this is because the spacecraft orbit periapses were near the south pole [18].

3 Theory Describing Lithospheric Flexure

According to the Airy model of isostasy, when a volcanic edifice forms above the crust, it is buoyantly supported and is compensated by a low-density crustal root, as seen in Figure 3. A characteristic low in the topography-corrected Bouguer anomaly is produced, caused by the negative density contrast between the mantle and the crustal root. Airy isostasy assumes a perfectly weak lithosphere that deforms readily and compensates all wavelengths of topography; however, it is more realistic to assign some effective elastic thickness T_e that represents the elastic strength of the lithosphere.

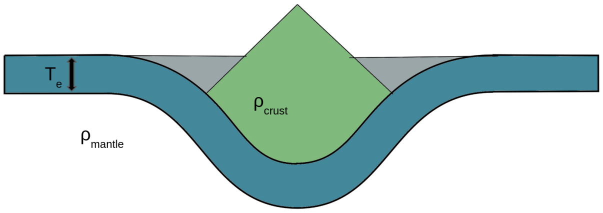

Figure 3: A topographic load is isostatically compensated at depth and produces a broad flexure of the crust-mantle boundary. The density contrast between the crust (ρ_c) and the mantle (ρ_m) results in a low in the Bouguer anomaly.

This elastic thickness serves to smooth out the compensating crust-mantle interface, reducing short-wavelength undulations. T_e has been shown on both Mars and Earth [32] to scale with lithospheric age, with younger, weaker crust having a smaller T_e than older crust. Subsurface loads, which may include dense intrusive material within or below the crust as well as mantle plumes [33, 34, 19, 7], may also contribute to flexure.

The magnitude of flexure, w, is positive in the downward direction and can be related to lithospheric properties using the differential equation that describes the balance of vertical forces,

$$D\nabla^4 w(x,y) + \Delta\rho g w(x,y) = \rho_c g h, \tag{1}$$

where D is the flexural rigidity, $\Delta\rho$ is the density contrast between the crust and the mantle, ρ_c is the crustal density, g is the acceleration of gravity on Mars (3.71 m/s^2), and h is the topography referenced to the ellipsoid. The flexural rigidity is,

$$D = \frac{ET_e^3}{12(1-\nu^2)}, \tag{2}$$

where E is Young's modulus, T_e is elastic thickness, and ν is Poisson's ratio. An analytical solution for w is produced by taking the Fourier transform of each term in Eq. 1 and solving for the Fourier transform of flexure $W(k)$,

$$W(k) = Q(k)H(k), \tag{3}$$

where k is wavenumber and the uppercase letters W and H denote the Fourier transforms of flexure and topography, respectively. $Q(k)$ is the linear transfer function for surface loading, and it is given by:

$$Q(k) = \frac{\rho_c g}{D\vec{K}^4 + \Delta\rho g} \tag{4}$$

The variable $\vec{K}$ is the two-dimensional wavenumber vector. Subsurface loading was neglected in this study. Eq. 3 provides an extremely convenient means of calculating the predicted flexure from topography.

4 Procedure

4.1 Low-Pass Filtering

Genova et al's (2016) degree strength model predicts a maximum resolution near Elysium to be around 85 degrees, corresponding to 125 km. However, this method relied on the Kaula Law constraint, which can result in an under-prediction in the gravity anomaly at large volcanoes [7]. Suspecting that the optimum resolution predicted by the degree strength method may thus be inaccurate, Broquet et al. (2019) define the maximum resolution to be where the localized spectral admittance and correlation significantly drop. At Elysium Rise, this occurs near 70 degrees, or a spatial resolution of 150 km. I test several cosine taper low-pass filters to remove spurious short-wavelength noise. The RMS error and variance of the residual anomaly are both expected to decrease steadily as higher degrees are removed, although overfiltering may remove real signal and influence the results. I find that filters with a maximum cutoff between 70 and 90 degrees and that taper over 5 degrees produce statistically identical results. To select a filter, I inspect the degree strength map produced by Genova et al. (2016), which indicates a maximum degree between 80 and 85 near the Elysium Rise. I adopt a slightly more conservative low-pass filter that is applied in the Fourier domain, which begins tapering at 75 degrees (wavelength = 283km) and cuts off all signal above 80 degrees (wavelength = 265km). Since the resolution of the MOLA topography is significantly higher than that of the GMM-3 gravity model, the topography grid must also be passed through this filter in order to match the resolution of the gravity.

4.2 Removal of Edge Effects

Edge effects introduced by Fourier-domain filtering can produce unwanted artifacts when the data is mapped in the spatial domain, making geologic interpretation difficult. Since both the free-air anomaly and topography maps are filtered, steps must be taken to counteract edge effects for both. To this end, I add buffer zones to the south and east of Elysium rise by linearly tapering the topography or free-air gravity anomaly values at each extended edge to those of the edge opposite from it. The resulting map is four times larger than the original, with opposite edges possessing equivalent values. The calculations of flexure and topographic correction described in this report are based on these buffered maps, although, as will be discussed later, the comparisons with observed gravity are performed over a smaller area neglecting the buffer zones.

4.3 Topographic (Bouguer) Correction

Multiple sources contribute to the raw gravity anomaly that must be corrected for in order to obtain the anomaly due to density variations. The first contributions that are normally corrected for are those of the planetary ellipsoid and of the effects of observation height. Both of these are corrected for in the GMM-3 free-air anomaly obtained from NASA's PDS Geoscience node, evaluated on the Martian ellipsoid. The free-air anomaly of the Elysium Volcanic Province is shown in Figure 4a. The free-air anomaly is dominated by the gravitational attraction of topography, which obscures the signal from the subsurface associated with flexure.

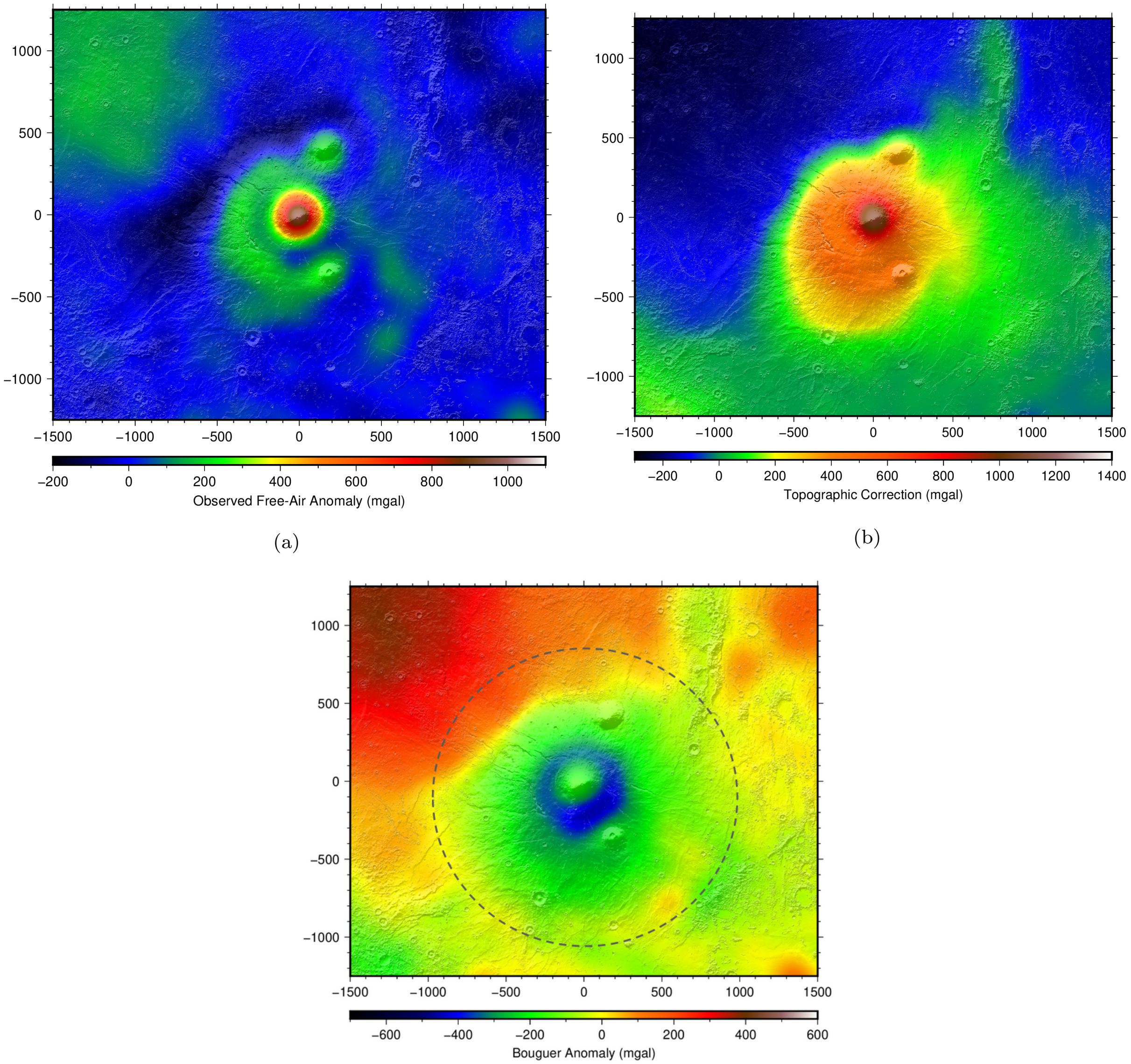

(a) (b)

(c)

Figure 4: (a) Observed free-air anomaly from the GMM-3 model. (b) Topographic (Bouguer) correction produced from MOLA topography. (c) Observed Bouguer anomaly produced by subtracting the Bouguer correction from the free-air anomaly.

I therefore correct for the topographic effects, g_z, using Parker's Fourier method [35],

$$g_z = \mathcal{F}^{-1}[2\pi\gamma\rho_c e^{-|\vec{K}|z_{obs}} \sum_{n=1}^{\infty} \frac{(-|\vec{K}|)^{n-1}}{n!} \mathcal{F}(h^n)], \tag{5}$$

where γ is the gravitational constant. In the calculation of the GMM-3 model, the gravity values were referenced to the ellipsoid, i.e. the Martian datum. The value for z_{obs} (the height of calculation) as used in the Parker sum, however, must be exterior to the mass involved in the calculation. Therefore, z_{obs} was taken to be the maximum topography. Truncating the infinite sum to five terms gives sufficiently high accuracy. Figure 4b shows the topographic correction for the Elysium Province. It can be seen that the topographic correction closely matches the topography of the region (Figure 1b). The Bouguer anomaly (Figure 4c) is produced by subtracting the topographic correction from the free-air anomaly. The Bouguer anomaly shows a broad negative anomaly (blue to green) that is associated with the downward flexure of the crust-mantle boundary due to the topographic load of the Elysium Rise.

4.4 Model Fitting and Statistics

The Bouguer anomaly that is predicted to result from the flexed crust-mantle boundary was calculated in a similar fashion to the topographic correction. Flexure was calculated using Eq. 2 through 4, and Eq. 5 was used to calculate the gravity signal due to the flexure. In this instance of Eq. 5, ρ_c is replaced with $\Delta\rho$, the density contrast between the crust and the mantle, and z_{obs} becomes the observation height with respect to the crust-mantle boundary; this latter value was obtained by summing the maximum topography height, the ambient crustal thickness (assumed to be 70 km), and the mean flexure. This was performed for values of T_e ranging from 0-100 km and for ρ_c from 2500-3400 kg/m^3. A mantle density of 3500 kg/m^3 was assumed. The range of T_e was chosen to extend beyond the range of T_e reported for Elysium Province in the literature, and densities were chosen to overlap with plausible load densities [36, 25, 26, 7] while including extreme low [37] and high values that approach mantle density. Each prediction was compared to the observed Bouguer anomaly for a given ρ_c by subtracting the prediction from the observation and removing the mean. The resulting residual gravity anomaly represents any subsurface density structure that deviates from the model structure, i.e. uniform crustal and mantle densities and a crust-mantle interface controlled by flexure. Both the RMS error and variance of the residual were calculated for the residual corresponding to each point in the T_e/ρ_c parameter space. Since Elysium Province sits on the edge of Utopia Basin, a massive, 4.1 Ga impact basin that possesses a very high Bouguer anomaly, only the portion of the residual within a 900 km radius of a point shifted 200 km south of the center of Elysium Mons was used in the calculation of the RMS error and variance. The radius and center of this circle (Figure 4c) were chosen in order to remove the Utopia Basin anomaly and focus on the three volcanoes of the Elysium Province. The forward-modelling, spatial-domain technique used here has the advantage over spectral localized admittance inversions of constraining crustal parameters while also allowing for geologic interpretation of anomalies in the residual gravity anomaly.

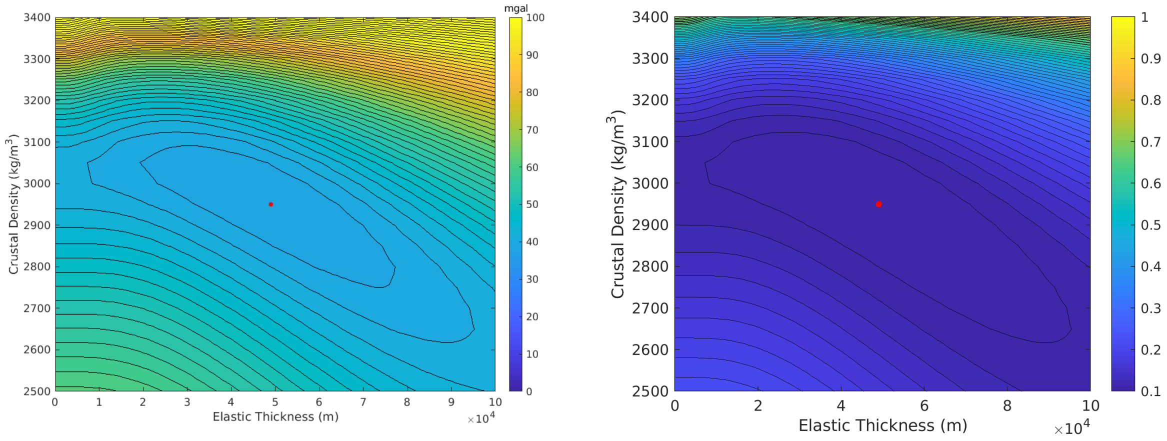

(a)

(b)

Figure 5: (a) RMS error of the residual gravity anomaly. (b) Variance of the residual gravity anomaly normalized to the variance of the free-air anomaly.

5 Results and Discussion

5.1 Elastic Thickness and Density

Figure 5 shows the RMS error and variance contour plots for the tested value ranges of T_e and ρ_c. Here, the variance parameter is normalized to the variance of the free-air anomaly and is computed within the circle shown in Figure 4c; it is formally the fraction of the observed signal that is not explained by the model. For example, a variance ratio of 0.1 means that 90% of the variance of the free-air anomaly is predicted by the model. The RMS error and variance fraction plots each exhibit a closed set of contours around a minimum, enabling best-fit values of T_e and ρ_c to be obtained. However, these minima are quite broad, and the best-fit values are not statistically unique. I adopt a maximum acceptable variance value of 0.1, which is the innermost contour of Figure 5b. Thus, anywhere within the T_e-ρ_c parameter space that lies within the innermost variance contour in Figure 5b constitutes a plausible set of solutions. For T_e, I thus obtain a range of 10 km to 90 km with a best-fit of 49 km, and for ρ_c I obtain values between 2650 kg/m^3 and 3100 kg/m^3 with a best-fit of 2950 kg/m^3. The range of T_e values mirrors the range found in the literature quite well, which is about 10 km to 50 km [22, 23, 24, 25, 26, 7, 27]; the lower bound of the best-fit range is consistent with the estimate of Broquet et al. (2019). The values obtained for ρ_c cover a wide range of possible densities, from very low bulk crustal estimates [37] to denser estimates for volcanic edifices (e.g., [26]).

5.2 Residual Gravity Anomaly

The map of the residual anomaly (Figure 6c) exposes a distinct, roughly circular high with a diameter of 300 km centered over Elysium Mons that is not explained by flexure. Explanations for its presence include it being a noise artifact, or it being the signature of a real subsurface density anomaly. The former scenario can be investigated by testing different cutoff wavelengths for the low-pass filters discussed above that are applied in

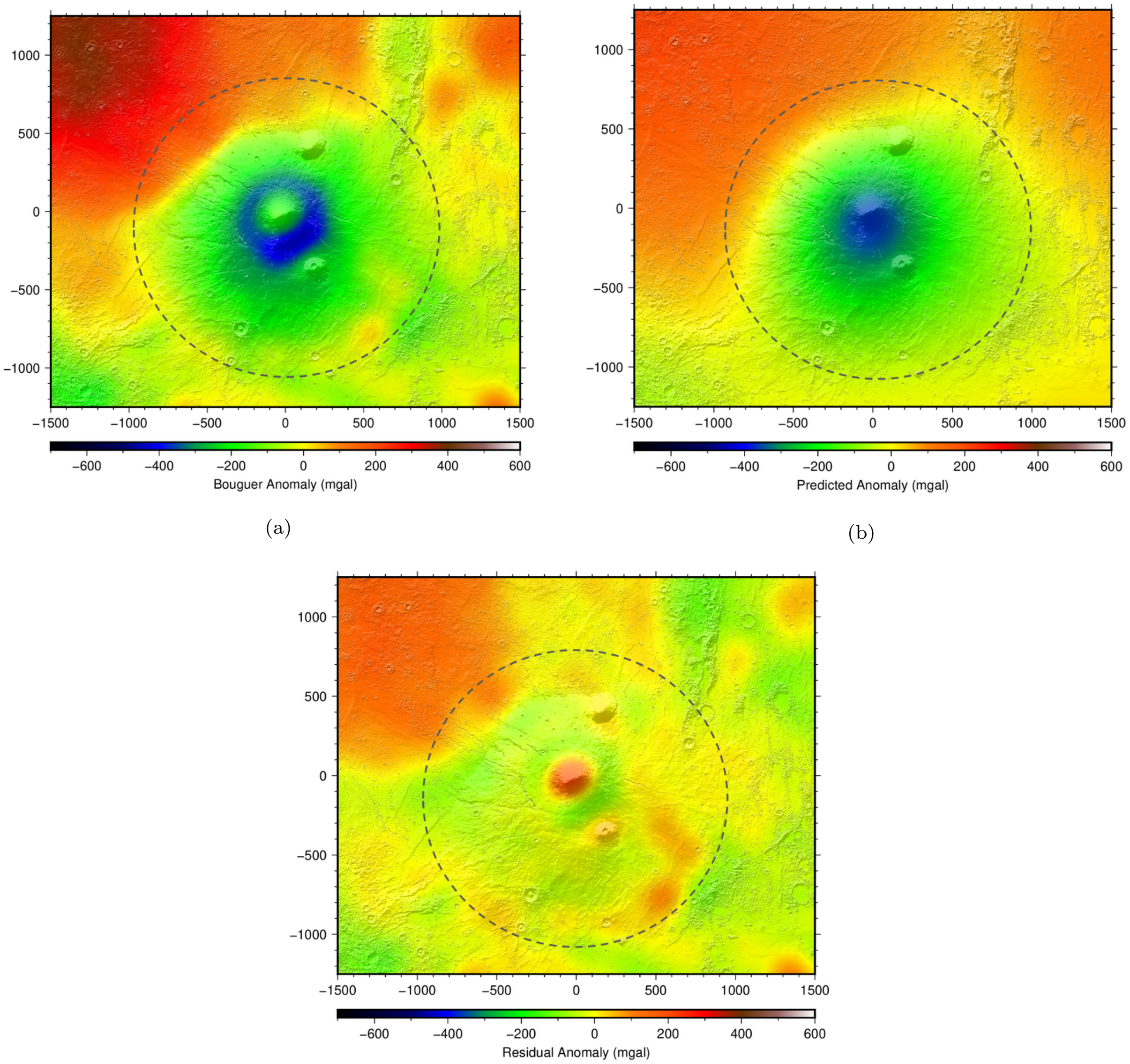

(a)

(b)

(c)

Figure 6: All three maps show the 900 km radius circle within which statistical analyses were performed. (a) Observed Bouguer anomaly produced by subtracting the topographic correction from the free-air anomaly. (b) Gravity anomaly predicted to result from flexure of the crust-mantle boundary. (c) Residual anomaly obtained by subtracting the observed gravity from the prediction.

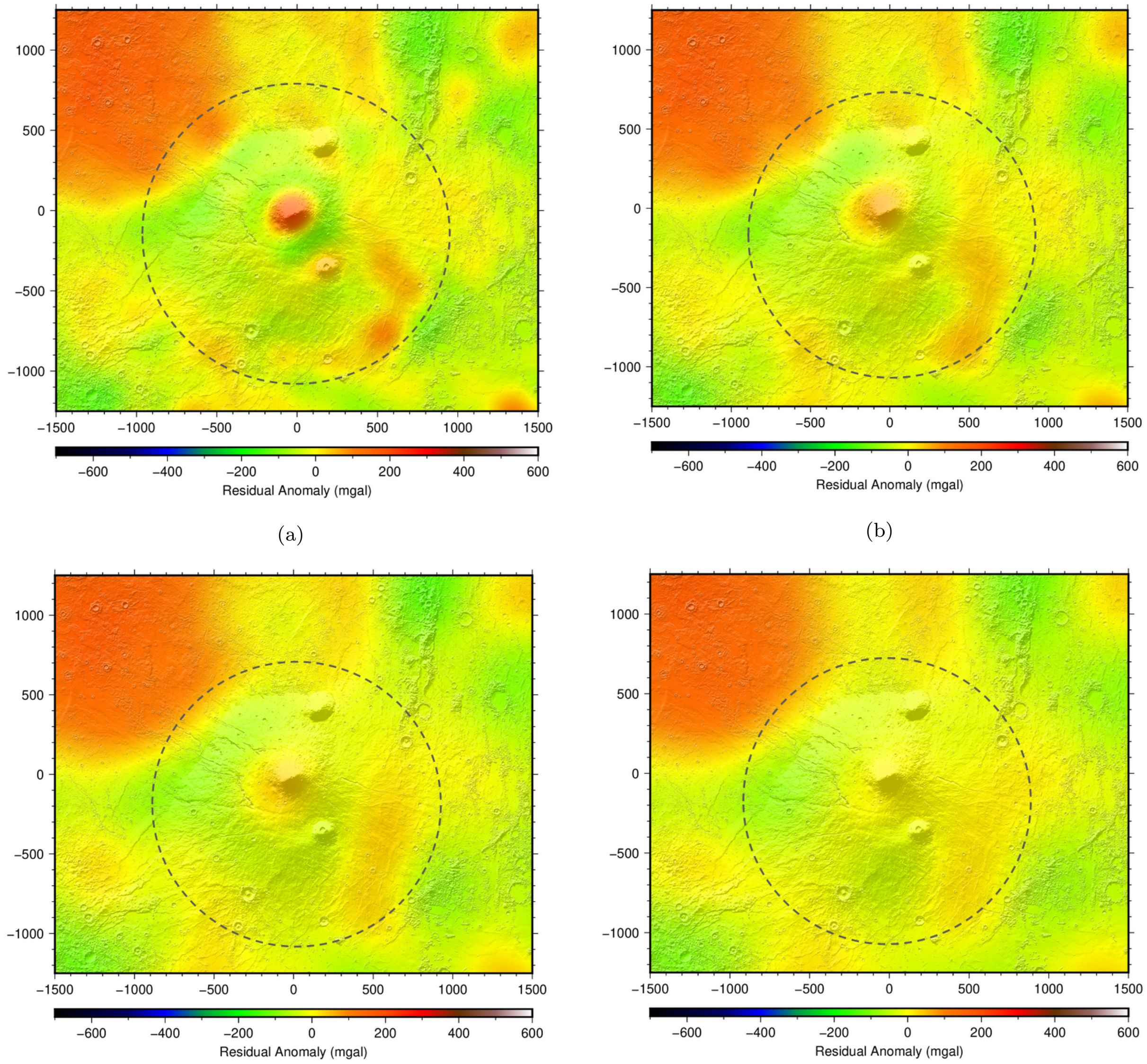

(a)

(b)

(c)

(d)

Figure 7: Residual anomalies for the best-fitting model ($T_e = 49$ km, $\rho_c = 2950$ kg/m^3) with low-pass Fourier filters applied with different maximum wavenumbers. (a) Spherical harmonic degrees above 80 removed (k = 0.0237 km^{-1}, resolution = 133 km), (b) above 50 degrees (k = 0.0149 km^{-1}, resolution = 211 km), (c) above 40 degrees (k = 0.0119 km^{-1}, resolution = 264 km), and (d) above 30 degrees (k = 0.0090 km^{-1}, resolution = 349 km).

the initial data processing steps. Different low-pass cosine taper filters were applied to the residual in order to test whether this feature is an artifact due to including spherical harmonic degrees beyond what is resolvable by the GMM-3 gravity model in the region. Figure 7 shows the residual with low-pass filters applied that remove wavelengths shorter than four cutoff values: 265 km (80 spherical harmonic degrees, Figure 7a), 423 km (50 degrees, Figure 7b), 527 km (40 degrees, Figure 7c), and 700 km (30 degrees, Figure 7d). Note that the smallest resolvable surface feature is half of the minimum wavelength in size. The anomaly can be seen to persist up to 40 degrees, which is well within the resolving power predicted by both Genova et al. (2016) and by Broquet et al. (2019). Furthermore, since the size of the anomaly is roughly 300 km, corresponding to a wavelength of 600 km, it is expected that the filter in Figure 7d should remove the anomaly, which it indeed does. These findings confirm that this anomaly is real and is not an artifact of poor gravity model resolution.

Positive gravity anomalies are commonly associated with shield volcanoes on Earth; these are the vestiges of extinct volcanic plumbing systems, long-cooled and filled with dense mafic cumulates, commonly olivines or pyroxenes. Such features in the gravity anomaly have also been identified on Mars and have also been attributed to extinct magma chambers [38, 39, 28]. While the gravity anomaly observed beneath Elysium Mons may be due to an underestimation of edifice density, the preferred interpretation is that it is the remnant of Elysium Mons' magmatic plumbing system.

To estimate the excess mass associated with the local gravity high, I first defined the "edge" of the anomaly as the contour where the residual is equal to zero. Gauss' Law as applied to gravity was then used to calculate the total mass contained within the defined boundary of the anomaly,

$$\int_{S_P} g_z dS = 2\pi\gamma M_T. \tag{6}$$

Here, the vertical component of gravity g_z, which is simply the value of the residual as derived from the GMM-3 model, is integrated over the surface bounded by the anomaly. Applying this method, I find the total mass contained within the anomaly to be $1.42 \cdot 10^{17}$ kg. This mass estimate is strikingly similar to Neumann et al.'s (2004) value of $1.19 \cdot 10^{17}$ kg, who performed a global analysis using an older, lower-resolution gravity model. The density estimate obtained for the Elysium Province ranges from 2650 kg/m^3 to 3100 kg/m^3; assuming igneous cumulates with an upper bound density of 3500 kg/m^3, these give density excesses between 850 kg/m^3 and 400 kg/m^3. These anomalous densities correspond to volume estimates of the magma chamber that are between $1.67 \cdot 10^{14}$ m^3 and $3.55 \cdot 10^{14}$ m^3. Using the optimal value of density obtained by this study, the volume is $2.58 \cdot 10^{14}$ m^3. For a spherical magma chamber, these volumes correspond to radii from 34.2 km to 43.9 km, with an optimal value of 39.5 km. A cylindrical magma chamber with a radius approximately the size of the gravity anomaly, 150 km, could have heights ranging from 2.36 km to 5.02 km, with an optimal height of 3.65 km. Overall, the dimensions of a spherical magma chamber would likely be much larger than the 14 km relief of Elysium Mons, although a cylindrical anomaly could have a vertical dimension on that scale or smaller.

6 Conclusions

In this work I used the recent GMM-3 gravity model of Mars and MOLA topography to constrain the effective elastic plate thickness of the lithosphere and crustal density beneath the Elysium Volcanic Province on Mars. These parameters are constrained to range between 10 km and 90 km and between 2650 kg/m^3 and 3100 kg/m^3, respectively, with best-fit values of 49 km and 2950 kg/m^3. These constraints are consistent with the ranges of values that have previously been reported in the literature for Elysium Mons using spectral admittance methods. In addition, a positive anomaly was identified robustly in the residual anomaly, which using Gauss' law is attributable to an excess mass of $1.42 \cdot 10^{17}$ kg. This excess mass is in agreement with the value obtained by Neumann et al. (2004) using a lower-resolution gravity model to within 20%. I also constrain the volume and possible dimensions of the anomaly, which I interpret to likely be a concentrated body of igneous cumulates representing the extinct magma chamber of Elysium Mons, similar to those found beneath shield volcanoes on Earth. I identify plausible volumes as being between $1.67 \cdot 10^{14}$ m^3 to $3.55 \cdot 10^{14}$ m^3. When applied to the case of a spherical magma chamber, these estimates indicate larger dimensions than Elysium Mons' 14 km relief and caldera.

6.1 Potential for Future Work

This project constitutes a successful application of Cartesian spatial analysis techniques to a region on Mars, typically used for Earth-based studies, and has potential for improved and expanded applications in future work. A significant improvement in the density determination could be made by differentiating between the density of the ambient crust and the internal density of the volcanic edifices using inverse techniques. With the latter hypothesized to be intrusive in origin, they likely are more ultramafic in nature with a higher density than the average ambient Martian crust (e.g., [6]). The spatial techniques used here could be applied to other features that have previously been too small to study using lower resolution gravity models. Small volcanoes as well as non-volcanic features such as impact craters or large rifts could be studied, many of which have not been studied extensively using gravity. Mars' south polar region is another potentially interesting target, since a large effective elastic thickness has been reported using an older, lower resolution gravity model [40]; since the GMM-3 model gives its highest resolution in this region, it could be used to update this value.

6.2 Acknowledgements

The MOLA topography and GMM-3 gravity model files used in this work were downloaded from NASA's Planetary Data System (PDS) Geosciences node. I would like to thank my advisors, Garrett Apuzen-Ito and Niels Grobbe, as well as my committee member Sarah Fagents, for guiding me through this project and for overall being helpful and encouraging.

References

[1] R. J. Stern, T. Gerya, and P. J. Tackley. Stagnant lid tectonics: Perspectives from silicate planets, dwarf planets, large moons, and large asteroids. *Geoscience Frontiers*, 9(1):103 – 119, 2018. Lid Tectonics.

[2] S. J. Robbins and B. M. Hynek. A new global database of Mars impact craters $\geq$1 km: 1. Database creation, properties, and parameters. *Journal of Geophysical Research: Planets*, 117(E5), 2012.

[3] S. J. Robbins, G. Di Achille, and B. M. Hynek. The volcanic history of Mars: High-resolution crater-based studies of the calderas of 20 volcanoes. *Icarus*, 211(2):1179 – 1203, 2011.

[4] T. Platz and G. Michael. Eruption history of the Elysium Volcanic Province, Mars. *Earth and Planetary Science Letters*, 312(1):140 – 151, 2011.

[5] M. H. Carr and R. Greeley. *Volcanic features of Hawaii: A basis for comparison with Mars*, volume 403. Scientific and Technical Information Branch, National Aeronautics and Space Administration, 1980.

[6] P. J. McGovern, S. C. Solomon, D. E. Smith, M. T. Zuber, M. Simons, M. A. Wieczorek, R. J. Phillips, G. A. Neumann, O. Aharonson, and J. W. Head. Localized gravity/topography admittance and correlation spectra on Mars: Implications for regional and global evolution. *Journal of Geophysical Research: Planets*, 107(E12):19–1–19–25, 2002.

[7] A. Broquet and M. A. Wieczorek. The Gravitational Signature of Martian Volcanoes. *Journal of Geophysical Research: Planets*, 124(8):2054–2086, 2019.

[8] M. Grott and D. Breuer. On the spatial variability of the Martian elastic lithosphere thickness: Evidence for mantle plumes? *Journal of Geophysical Research: Planets*, 115(E3), 2010.

[9] A.-C. Plesa, S. Padovan, N. Tosi, D. Breuer, M. Grott, M. A. Wieczorek, T. Spohn, S. E. Smrekar, and W. B. Banerdt. The Thermal State and Interior Structure of Mars. *Geophysical Research Letters*, 45(22):12,198–12,209, 2018.

[10] D. E. Smith, M. T. Zuber, H. V. Frey, J. B. Garvin, J. W. Head, D. O. Muhleman, G. H. Pettengill, R. J. Phillips, S. C. Solomon, H. J. Zwally, W. B. Banerdt, T. C. Duxbury, M. P. Golombek, F. G. Lemoine, G. A. Neumann, D. D. Rowlands, O. Aharonson, P. G. Ford, A. B. Ivanov, C. L. Johnson, P. J. McGovern, J. B. Abshire, R. S. Afzal, and X. Sun. Mars Orbiter Laser Altimeter: Experiment summary after the first year of global mapping of Mars. *Journal of Geophysical Research: Planets*, 106(E10):23689–23722, 2001.

[11] J. P. Gapcynski, R. H. Tolson, and W. H. Michael Jr. Mars gravity field: Combined Viking and Mariner 9 results. *Journal of Geophysical Research (1896-1977)*, 82(28):4325–4327, 1977.

[12] J. Lorell, G. H. Born, E. J. Christensen, P. B. Esposito, J. Frank Jordan, P. A. Laing, W. L. Sjogren, S. K. Wong, R. D. Reasenberg, I. I. Shapiro, and G. L. Slater. Gravity Field of Mars from Mariner 9 Tracking Data (A. 6.2 and A. 6. 1). *Icarus*, 18(2):304–316, February 1973.

[13] W. L. Sjogren, J. Lorell, L. Wong, and W. Downs. Mars gravity field based on a short-arc technique. *Journal of Geophysical Research (1896-1977)*, 80(20):2899–2908, 1975.

[14] D. Smith, W. Sjogren, G. Tyler, G. Balmino, F. Lemoine, and A. Konopliv. The Gravity Field of Mars: Results from Mars Global Surveyor. *Science (New York, N.Y.)*, 286:94–7, 11 1999.

[15] A. S. Konopliv, C. F. Yoder, E. M. Standish, D.-N. Yuan, and W. L. Sjogren. A global solution for the Mars static and seasonal gravity, Mars orientation, Phobos and Deimos masses, and Mars ephemeris. *Icarus*, 182(1):23 – 50, 2006.

[16] A. S. Konopliv, S. W. Asmar, W. M. Folkner, Ö. Karatekin, D. C. Nunes, S. E. Smrekar, C. F. Yoder, and M. T. Zuber. Mars high resolution gravity fields from MRO, Mars seasonal gravity, and other dynamical parameters. *Icarus*, 211(1):401 – 428, 2011.

[17] A. S. Konopliv, R. S. Park, and W. M. Folkner. An improved JPL Mars gravity field and orientation from Mars orbiter and lander tracking data. *Icarus*, 274:253 – 260, 2016.

[18] A. Genova, S. Goossens, F. G. Lemoine, E. Mazarico, G. A. Neumann, D. E. Smith, and M. T. Zuber. Seasonal and static gravity field of Mars from MGS, Mars Odyssey and MRO radio science. *Icarus*, 272:228 – 245, 2016.

[19] P. Audet. Toward mapping the effective elastic thickness of planetary lithospheres from a spherical wavelet analysis of gravity and topography. *Physics of the Earth and Planetary Interiors*, 226:48 – 82, 2014.

[20] W. S. Kiefer and B. H. Hager. The Role of Mantle Convection in the Origin of the Tharsis and Elysium Provinces of Mars. In *MEVTV Workshop on Early Tectonic and Volcanic Evolution of Mars*, pages 48–50, January 1989.

[21] A.-C. Plesa, M. Grott, N. Tosi, D. Breuer, T. Spohn, and M. A. Wieczorek. How large are present-day heat flux variations across the surface of Mars? *Journal of Geophysical Research: Planets*, 121(12):2386–2403, 2016.

[22] R. P. Comer, S. C. Solomon, and J. W. Head. Mars: Thickness of the lithosphere from the tectonic response to volcanic loads. *Reviews of Geophysics*, 23(1):61–92, 1985.

[23] J. L. Hall, S. C. Solomon, and J. W. Head. Elysium Region, Mars: Tests of lithospheric loading models for the formation of tectonic features. *Journal of Geophysical Research: Solid Earth*, 91(B11):11377–11392, 1986.

[24] D. McKenzie, D. N. Barnett, and D.-N. Yuan. The relationship between Martian gravity and topography. *Earth and Planetary Science Letters*, 195(1):1 – 16, 2002.

[25] P. J. McGovern, S. C. Solomon, D. E. Smith, M. T. Zuber, M. Simons, M. A. Wieczorek, R. J. Phillips, G. A. Neumann, O. Aharonson, and J. W. Head. Correction to "Localized gravity/topography admittance and correlation spectra on Mars: Implications for regional and global evolution". *Journal of Geophysical Research: Planets*, 109(E7), 2004.

[26] V. Belleguic, P. Lognonné, and M. Wieczorek. Constraints on the Martian lithosphere from gravity and topography data. *Journal of Geophysical Research: Planets*, 110(E11), 2005.

[27] M. Ding, J. Lin, C. Gu, Q. Huang, and M. T. Zuber. Variations in Martian Lithospheric Strength Based on Gravity/Topography Analysis. *Journal of Geophysical Research: Planets*, 124(11):3095–3118, 2019.

[28] G. A. Neumann, M. T. Zuber, M. A. Wieczorek, P. J. McGovern, F. G. Lemoine, and D. E. Smith. Crustal structure of Mars from gravity and topography. *Journal of Geophysical Research: Planets*, 109(E8), 2004.

[29] W. M. Kaula. Determination of the Earth's gravitational field. *Reviews of Geophysics*, 1(4):507–551, 1963.

[30] A. I. Ermakov, R. S. Park, and B. G. Bills. Power Laws of Topography and Gravity Spectra of the Solar System Bodies. *Journal of Geophysical Research: Planets*, 123(8):2038–2064, 2018.

[31] E. Mazarico, A. Genova, S. Goossens, F. G. Lemoine, G. A. Neumann, M. T. Zuber, D. E. Smith, and S. C. Solomon. The gravity field, orientation, and ephemeris of Mercury from MESSENGER observations after three years in orbit. *Journal of Geophysical Research: Planets*, 119(12):2417–2436, 2014.

[32] A.B. Watts, S.J. Zhong, and J. Hunter. The Behavior of the Lithosphere on Seismic to Geologic Timescales. *Annual Review of Earth and Planetary Sciences*, 41(1):443–468, 2013.

[33] D. W. Forsyth. Subsurface loading and estimates of the flexural rigidity of continental lithosphere. *Journal of Geophysical Research: Solid Earth*, 90(B14):12623–12632, 1985.

[34] G. Ito and A. Taira. Compensation of the Ontong Java Plateau by surface and subsurface loading. *Journal of Geophysical Research: Solid Earth*, 105(B5):11171–11183, 2000.

[35] R. L. Parker. The Rapid Calculation of Potential Anomalies. *Geophysical Journal International*, 31(4):447–455, 03 1973.

[36] M. T. Zuber, S. C. Solomon, R. J. Phillips, D. E. Smith, G. L. Tyler, O. Aharonson, G. Balmino, W. B. Banerdt, J. W. Head, C. L. Johnson, F. G. Lemoine, P. J. McGovern, G. A. Neumann, D. D. Rowlands, and S. Zhong. Internal Structure and Early Thermal Evolution of Mars from Mars Global Surveyor Topography and Gravity. *Science*, 287(5459):1788–1793, 2000.

[37] S. Goossens, T. J. Sabaka, A. Genova, E. Mazarico, J. B. Nicholas, and G. A. Neumann. Evidence for a low bulk crustal density for Mars from gravity and topography. *Geophysical Research Letters*, 44(15):7686–7694, 2017.

[38] W. Kiefer. Gravity Evidence for Extinct Magma Chamber Systems on Mars. *Sixth International Conference on Mars*, 07 2003.

[39] W. S. Kiefer. Gravity evidence for an extinct magma chamber beneath Syrtis Major, Mars: a look at the magmatic plumbing system. *Earth and Planetary Science Letters*, 222(2):349 – 361, 2004.

[40] M. A. Wieczorek. Constraints on the composition of the martian south polar cap from gravity and topography. *Icarus*, 196(2):506 – 517, 2008. Mars Polar Science IV.